

# Laser-cluster interaction in an external magnetic field: the effect of laser polarization

Kalyani Swain<sup>1,2</sup> and Mrityunjay Kundu<sup>1,2</sup>

<sup>1</sup>*Institute for Plasma Research, Bhat, Gandhinagar, 382428, India*

<sup>2</sup>*Homi Bhabha National Institute, Training School Complex, Anushaktinagar, Mumbai 400094, India*

(Dated: May 27, 2024)

Collisionless absorption of laser energy by an electron via laser-cluster interaction in an ambient magnetic field ( $B_0$ ) has recently renewed interest. Previously, using a rigid sphere model (RSM) and an extensive particle-in-cell (PIC) simulation with linearly polarized (LP) laser light, we have shown that an auxiliary field  $B_0$  in a transverse direction to the laser polarization significantly enhances the laser absorption [Scientific Reports **12**, 11256 (2022)]. In this LP case, the average energy ( $\mathcal{E}_A$ ) of an electron rises near 30 – 70 times of its ponderomotive energy ( $U_p$ ). The two-stage laser absorption by cluster electrons has been attributed via anharmonic resonance (AHR) followed by electron-cyclotron resonance (ECR) satisfying the improved phase-matching and frequency-matching conditions simultaneously. In the present work, we study the effect of circularly polarized (CP) laser fields on the cluster-electron dynamics considering left/right circular polarizations with an ambient  $B_0$ . In typical conditions, without  $B_0$ , we show that both LP and CP light yield almost the same level of laser absorption (about  $3U_p$  or less) by an electron. However, with  $B_0$ , CP light enhances the electron's energy *further* by  $\approx 10 - 20U_p$  beyond the previously reported values  $\approx 30 - 70U_p$  by the LP light. These ejected electrons from cluster show narrow cone-like propagation as a weakly relativistic electron beam with an angular spread  $\Delta\theta < 5^\circ$  and the beam quality improves in CP than LP. In all cases, RSM and PIC results show good agreement.

## I. INTRODUCTION

In the past few decades, table-top size particle accelerators based on laser-plasma interaction have brought significant progress to replace a traditional multi-kilometer high-energy particle accelerator. The production of a relativistic electron beam (REB) via laser-plasma interaction is also of current interest due to its many applications, e.g., in the fast ignition technique of inertial confinement fusion and medical fields. Here target material plays an important role. As a unique target media, atomic nano-clusters with solid-like local density may absorb nearly 80% of laser energy compared to bulk solid and gas targets<sup>1</sup>. Laser-cluster interaction (LCI) may produce energetic ions<sup>1-4</sup>, neutrals<sup>5</sup>, electrons<sup>2,6-9</sup> and x-rays<sup>10-14</sup>, thereby opening avenues for new-generation particle accelerators and light sources. The fundamental processes involved in LCI encompass: (i) inner ionization —separation of electrons (and ions) from parent atom, results the generation of nano-plasma, (ii) outer ionization —complete removal of electrons from the cluster boundary, (iii) coulomb explosion —expansion of the ionic background which are discussed in earlier works<sup>15-18</sup>.

In the collision-less regime of laser absorption<sup>19-22</sup> by cluster electrons (for laser intensities  $I_0 > 10^{16}$  W/cm<sup>2</sup> and wavelength  $\lambda > 600$  nm), linear resonance (LR) and anharmonic resonance (AHR) are significant. The LR occurs<sup>23-26</sup> for a long-duration laser pulse (typically  $> 50$  fs) when there is sufficient coulomb explosion of the cluster (which is over-dense initially;  $\rho_i > \rho_c$ ). This happens as the charge density of ions  $\rho_i(t)$  eventually decreases and meets the critical plasma density  $\rho_c = \omega^2/4\pi$ , where the dynamic Mie-plasma frequency  $\omega_M(t) = \sqrt{4\pi\rho_i/3}$  aligns with the laser frequency  $\omega = 2\pi c/\lambda$ . We use atomic units (a.u.) where  $|e| = m_0 = \hbar = 4\pi\epsilon_0 = 1$  unless noted explicitly. On the other

hand, for short duration laser pulse, LR can not happen since cluster is over-dense with  $\omega_M(t) > \omega$ , and in this case AHR plays important role. During AHR, the self-consistent anharmonic potential of the cluster allows the electron oscillation frequency to dynamically align with  $\omega$ . Significance of AHR is discussed frequently in numerous studies<sup>27-33</sup> using a simple rigid sphere model (RSM) of cluster, particle-in-cell (PIC) and molecular dynamics (MD) simulations.

A comprehensive review for LCI, as given in Table-I of Ref.<sup>34</sup>, reveals an interesting observation without an external magnetic field  $B_0$ . It shows that, even when the laser has an adequate supply of energy, the maximum average energy attained by a cluster electron mostly remains close to  $\approx 3.17U_p$  (similar to the laser-atom<sup>35-37</sup> interaction) or below. Here,  $U_p = I_0/4\omega^2$  is the non-relativistic ponderomotive energy of an electron. In Ref.<sup>34</sup>, using RSM and a three-dimensional PIC simulation, we show that an ambient magnetic field ( $B_0$ ) in transverse orientation to the linearly polarized laser field of a 5-fs broadband laser pulse (with  $\lambda = 800$  nm and intensities  $I_0 \approx 10^{16} - 10^{18}$  W/cm<sup>2</sup>) can significantly enhance average energy of an electron  $\mathcal{E}_A$  up to  $\approx 36 - 70U_p$  (more than 12 – 36 fold) while interacting with a deuterium cluster. This substantial improvement in laser energy absorption is a two stage process: with AHR as the *first stage* and electron cyclotron resonance (ECR) or relativistic ECR (RECR) as the *second stage*, where electron cyclotron frequency  $\Omega_c = |e|B_0/m_0\gamma = \Omega_{c0}/\gamma$  meets the laser frequency  $\omega$  and simultaneously satisfies the phase matching condition. In a subsequent work<sup>38</sup> we increase the cluster size ( $R_0 \approx 2.2 \rightarrow 4.4$  nm) and show that, under similar conditions, per electron energy  $\mathcal{E}_A$  remains almost the same ( $\approx 36 - 70U_p$ ) near ECR, but in the regime of 100% outer-ionization (at high intensities) the net absorption increases almost linearly with the number of electrons ( $N$ ). We find that laser-coupled cluster electrons form a nearly

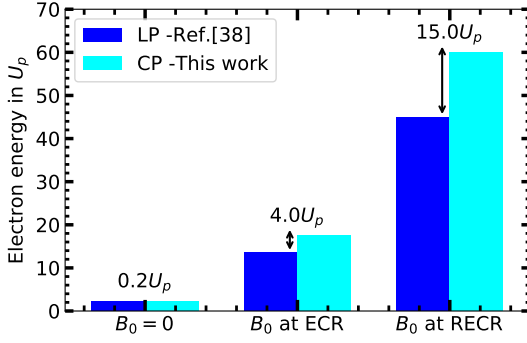


Figure 1. Schematic of comparison of average energy gain by a laser-driven cluster-electron for LP and CP fields with/without  $B_{ext}$ .

mono-energetic weakly relativistic, spirally narrow beam that traverses a few hundred of  $R_0$  (or on the order of  $\lambda$ ) with momentum  $p/m_0c > 1.7$  in an ambient magnetic field near ECR, which may not be possible only with the laser field. Also, as the cluster size increases, the intensity of electron beam increases with a greater number of energetic electrons at a restricted angle of  $\theta_r \approx 7^\circ - 10^\circ$  (in the position space) and  $\theta_p \approx 58^\circ - 62^\circ$  (in the momentum space) w.r.t. the laser propagation direction  $\mathbf{z}$  for  $I_0 = 7.13 \times 10^{16} - 1.83 \times 10^{17} \text{ W/cm}^2$ .

In this paper we study the effect of circular polarized (CP) laser field on the energy absorption and subsequent dynamics of cluster electrons in presence of an ambient magnetic field  $\mathbf{B}_{ext} = \pm B_0 \hat{\mathbf{z}}$  using RSM and PIC simulations. We show that, for CP laser fields absorbed energy per electron  $\mathcal{E}_A$  is further enhanced and it is  $10 - 20 U_p$  more compared to the linearly polarized (LP) cases<sup>34,38</sup>. To provide a quick summary, in Figure 1 we show a schematic of comparison of average energy gain by a laser-driven cluster-electron for LP and CP fields with/without  $B_{ext}$  for  $I_0 = 1.83 \times 10^{17} \text{ W/cm}^2$ . Additionally, we find that right circular polarized (RCP) and left circular polarized (LCP) laser fields yield the same amount of absorption, but the direction of  $\mathbf{B}_{ext}$  for LCP (RCP) should be along  $-\hat{\mathbf{z}}$  ( $+\hat{\mathbf{z}}$ ) w.r.t. laser propagation direction. Note that the field components of a CP light does not vanish simultaneously, while for LP it can reach zero. The phase matching condition show that one of the field components with CP light may maintain the required phase with non-zero amplitude. This leads to higher absorption of the CP laser pulse than the LP case in presence of  $\mathbf{B}_{ext}$ . In addition, we find that the quality of the emitted electron beam in terms of divergence and energy is improved in CP than LP.

In Sec.II laser pulse and cluster parameters are introduced. In Sec.III we describe RSM and PIC method followed by the simulation results. In Sec.IV we summarize this work.

## II. LASER PULSE AND CLUSTER PARAMETERS

We assume a laser pulse<sup>34,39,40</sup> propagating in  $\mathbf{z}$  with a vector potential

$$\mathbf{A}(t') = \frac{E_0}{\omega} \sin^2 \left( \frac{\omega t'}{2n} \right) \left[ \delta \cos(\omega t') \hat{\mathbf{x}} + \sqrt{1 - \delta^2} \sin(\omega t') \hat{\mathbf{y}} \right]. \quad (1)$$

Where  $t' = t - z/c$  is the retarded time,  $\tau = nT$  is the pulse duration such that  $0 \leq t' \leq \tau$ , and  $n$  is the number of laser

period  $T$ . The factor  $\delta = 1$  is for LP with polarization in  $\mathbf{x}$ , and  $\delta = \pm 1/\sqrt{2}$  are for left/right CP (LCP/RCP) respectively. The field strength is  $E_0 = \sqrt{I_0}$ . Laser electric and magnetic fields  $\mathbf{E}_l, \mathbf{B}_l$  are obtained from

$$\mathbf{E}_l(t') = -\frac{\partial \mathbf{A}}{\partial t}, \quad \mathbf{B}_l(t') = \hat{\mathbf{z}} \times \mathbf{E}_l(t')/c. \quad (2)$$

The laser pulses (1) show broad-band nature (for short pulses) due to three discrete frequencies  $\omega_1 = \omega, \omega_2 = (1 + 1/n)\omega, \omega_3 = (1 - 1/n)\omega$ . We assume  $\lambda = 800 \text{ nm}$ ,  $n = 5$ , and  $\tau = nT \approx 13.5 \text{ fs}$  ( $\tau_{fwhm} \sim 5 \text{ fs}$ ) in this work.

A deuterium cluster of number of atoms  $N = 2176$  is chosen. With the Wigner-Seitz radius  $r_w \approx 0.17 \text{ nm}$ , cluster radius is  $R_0 = r_w N^{1/3} \approx 2.2 \text{ nm}$ . Since  $R_0 \ll \lambda$ , the dipole approximation  $z/\lambda \ll 1$  may be assumed. For  $\lambda = 800 \text{ nm}$  laser, the critical density is  $\rho_c \approx 1.75 \times 10^{27} \text{ m}^{-3}$ . Hence, the cluster is  $\rho_i/\rho_c \approx 27.1$  times overdense with  $(\omega_M/\omega)^2 \approx 9.1$ .

## III. MODEL AND NUMERICAL SIMULATIONS

We pursue two numerical approaches in this work, namely a simple RSM and self-consistent PIC simulation. These are already described in earlier works<sup>29,30,34,38</sup>. Therefore, we describe them in short to maintain the readability.

### A. Rigid sphere model (RSM)

The rigid sphere model (RSM) simplifies the description of the dynamics of an electron in the case of laser-cluster interaction. It also provides a useful framework for understanding many physics aspects of laser absorption. In this model, cluster is considered as a pre-ionized nano-plasma which is spherical in shape. For simplicity, the ionic background is considered to be of the same as that of the initial cluster radius  $R_0$ . As we focus on the short-pulse laser duration, the ions are treated as stationary (or frozen) and their dynamics are omitted in the RSM. The ionic charge density  $\rho_i = 3NZ/4\pi R_0^3$  defines the Mie-plasma frequency  $\omega_M^2 = 4\pi\rho_i/3$  for fully ionized number of atoms  $N$  each of charge  $Z = 1$ . RSM is widely discussed in earlier works<sup>27-30,33,34,40-42</sup> which include the dynamics of a single electron as well as non-interacting multi-electrons to mimic a more realistic scenario. The potential  $\Phi_l(r)$  and the space-charge field  $\mathbf{E}_{sc}(\mathbf{r})$  in RSM are given by

$$\phi_l(r) = \omega_M^2 R_0^2 \begin{cases} 3/2 - r^2/2R_0^2 \\ R_0/r \end{cases}; \quad \mathbf{E}_{sc}(\mathbf{r}) = \begin{cases} \omega_M^2 \mathbf{r} \\ \omega_M^2 R_0^3 \mathbf{r}/r^3 \end{cases} \quad (3)$$

The top and bottom lines are for  $r \leq R_0$  and  $r > R_0$  respectively. An electron interacts with the applied fields  $(\mathbf{E}_l, \mathbf{B}_l)$ , and  $\mathbf{B}_{ext}$  including the coulomb field  $E_{sc}(r)$  obeying the following equations

$$\frac{d\mathbf{p}}{dt} = q[(\mathbf{E}_l + \mathbf{E}_{sc}(\mathbf{r})) + \mathbf{v} \times (\mathbf{B}_l + \mathbf{B}_{ext})] \quad (4)$$

$$\frac{d\mathbf{r}}{dt} = \mathbf{v} = \frac{\mathbf{p}}{\gamma m_0} \quad (5)$$

$$\frac{d(\gamma m_0 c^2)}{dt} = q\mathbf{v} \cdot (\mathbf{E}_l + \mathbf{E}_{sc}(\mathbf{r})) \quad (6)$$

where  $\gamma = 1/\sqrt{1-v^2/c^2} = \sqrt{1+p^2/m_0^2c^2}$  is the relativistic  $\gamma$ -factor for the electron.  $m_0, q, \mathbf{r}, \mathbf{v}, \mathbf{p}$  are the rest-mass ( $m_0 = 1$  in a.u.), charge ( $q = e = -1$  in a.u.), position, velocity and linear momentum respectively. In earlier works<sup>34,38</sup>, we have demonstrated that the average energy absorption of multiple non-interacting electrons in the RSM in an ambient magnetic field is very similar to that of a single electron in RSM. Hence, we do not reiterate those RSM results with multiple non-interacting electrons here. Instead, we consider a single electron in the RSM when exposed to a CP light and compare the RSM results with the self-consistent PIC results.

### 1. Laser absorption by an electron with LP and CP laser field

In the previous works<sup>34,38</sup> we studied interaction of LP laser pulses with deuterium clusters in presence of ambient magnetic fields in the range of  $|\mathbf{B}_{ext}| = |B_0\hat{z}| = 0 - 20$  kT. The intensity of LP pulses were  $I_0 \approx 7 \times 10^{16} - 2 \times 10^{17} \text{ W/cm}^2$  with fixed wavelength 800 nm and pulse duration of  $\sim 13$  fs. The average energy absorption by an electron was enhanced in the range of  $\overline{\mathcal{E}}_A \approx 35 - 70U_p$  due to ECR (where,  $\Omega_c = \Omega_{c0} = \omega$ ) for  $|\mathbf{B}_{ext}| = |B_0\hat{z}| = 0 - 20$  kT from a value of  $\overline{\mathcal{E}}_A \approx 2U_p$  (or below) without  $\mathbf{B}_{ext}$ . Note that, in those cases  $\mathbf{B}_{ext} = B_0\hat{z}$  were chosen along the laser propagation  $+\hat{z}$ . However, the dynamics of cluster electrons for a reversed  $\mathbf{B}_{ext} = -B_0\hat{z}$  is still not addressed for the LP light. The effect of CP laser fields with  $\mathbf{B}_{ext} = \pm B_0\hat{z}$  and corresponding ECR absorption have not been reported so far for laser-cluster interaction.

In Figure 2 we compare the temporal variation of normalized absorbed energy ( $\overline{\mathcal{E}}_A = \mathcal{E}_A/U_p$ ) by a single electron in the RSM with LP (Fig.2a) and CP (Fig.2b) laser fields for two opposite orientations of  $\mathbf{B}_{ext} = \pm B_0\hat{z}$ . The CP cases include left/right circular polarizations (LCP/RCP). The laser-pulse is  $n = 5$ -cycle as in Eq.(1) with intensity  $I_0 = 1.83 \times 10^{17} \text{ W/cm}^2$ . The electron is initially placed at the center of the cluster with zero velocity. When no external magnetic field ( $B_0 = 0$ ), energy absorption by the electron is  $\overline{\mathcal{E}}_A \approx 0.5$  for all cases of LP and CP, in the end of the pulses. However, in the presence of an ambient magnetic field at the ECR value of  $B_0 = \omega = 0.057$  a.u. ( $\approx 13$  kilo Tesla) with LP laser we obtain  $\overline{\mathcal{E}}_A \sim 13$  for  $\mathbf{B}_{ext} = \pm B_0\hat{z}$  (solid and dashed-dot, Fig.2a). It means that the value of absorption  $\overline{\mathcal{E}}_A$  is unaltered irrespective of the orientation of  $\mathbf{B}_{ext} = \pm B_0\hat{z}$  for the LP light.

At the ECR value of  $B_0 = \omega = 0.057$  a.u., when  $\mathbf{B}_{ext} = +B_0\hat{z}$ , the energy  $\overline{\mathcal{E}}_A$  is enhanced up to  $\approx 17$  for RCP (dashed-dot); and for  $\mathbf{B}_{ext} = -B_0\hat{z}$ , absorption drops to  $\overline{\mathcal{E}}_A \approx 0.5$  as without  $\mathbf{B}_{ext}$  for RCP (Fig.2b). For LCP with  $\mathbf{B}_{ext} = -B_0\hat{z}$  we obtain equal amount of enhancement in  $\overline{\mathcal{E}}_A \approx 17$  (solid, light-grey) similar to the RCP with  $\mathbf{B}_{ext} = +B_0\hat{z}$ . Again, when  $\mathbf{B}_{ext} = +B_0\hat{z}$  for LCP laser, the absorption drops to  $\overline{\mathcal{E}}_A \approx 0.5$  as without  $\mathbf{B}_{ext}$ . Clearly, laser absorption depends on the orientation of  $\mathbf{B}_{ext}$  for RCP/LCP laser fields. In short, RCP favours  $\mathbf{B}_{ext} = +B_0\hat{z}$  and LCP favours  $\mathbf{B}_{ext} = -B_0\hat{z}$  for the electron's energy enhancement due to the co-rotating cyclotron motions with these respective CP fields. Importantly, the value of  $\overline{\mathcal{E}}_A$  is more than  $4U_p$  higher in the end of the laser pulse, for both RCP/LCP fields than the respective LP cases at the ECR.

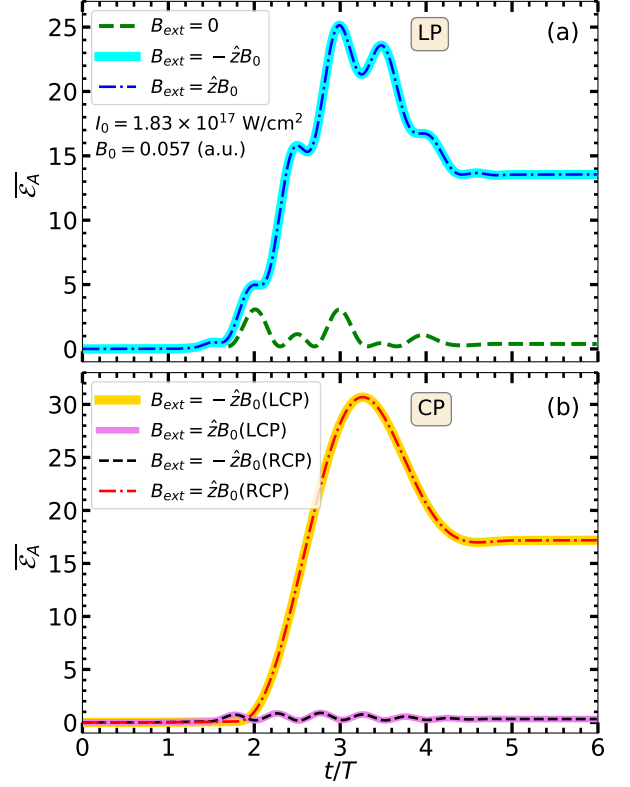


Figure 2. Time vs total laser energy absorption  $\overline{\mathcal{E}}_A$  in  $U_p$  for a single electron in RSM for (a) LP laser when  $\mathbf{B}_{ext} = \pm B_0\hat{z}$  (blue dash-dot and cyan solid lines; black dash-dot and light grey solid lines in grey scale), and  $\mathbf{B}_{ext} = 0$  (green dashed line; dark grey dashed lines in grey scale), (b) RCP laser field when  $\mathbf{B}_{ext} = \pm B_0\hat{z}$  (dash-dot red, dashed black lines; dark grey dash-dot and black dashed lines in grey scale), and LCP laser field when  $\mathbf{B}_{ext} = \pm B_0\hat{z}$  (purple and yellow solid lines; dark grey and light grey solid lines in grey scale). Here  $B_0 = 0.057 \text{ a.u.} = 13.37 \text{ kT}$  and intensity  $I_0 = 1.83 \times 10^{17} \text{ W/cm}^2$ .

In the case of LP laser,  $\overline{\mathcal{E}}_A$  is shown (Fig. 2) unaltered irrespective of the orientation  $\mathbf{B}_{ext} = \pm B_0\hat{z}$ , but the corresponding electron dynamics may differ as shown in Fig.3. The electron dynamics in  $x, z$  do not change for  $\mathbf{B}_{ext} = \pm B_0\hat{z}$  in the position and the momentum space (Fig.3a1, 3a2). However, the dynamics in  $y$ -direction in both position and in momentum space are in opposite phase for  $\mathbf{B}_{ext} = \pm B_0\hat{z}$ . It shows clockwise rotation for  $\mathbf{B}_{ext} = +B_0\hat{z}$  and anticlock-wise rotation for  $\mathbf{B}_{ext} = -B_0\hat{z}$  in the  $x$ - $y$  plane, but the electron always moves forward in  $\hat{z}$ .

The trajectory of the electron in the position and momentum space (Fig. 3b1,3b2) for LCP field with  $\mathbf{B}_{ext} = -B_0\hat{z}$  resembles with the LP case when  $\mathbf{B}_{ext} = -B_0\hat{z}$  and the RCP case resembles with the LP case when  $\mathbf{B}_{ext} = +B_0\hat{z}$ . However, the amplitude of respective trajectories are different for LP and CP fields, particularly  $z, p_z$  are higher for CP than LP. The higher  $p_z$  explains higher energy for the CP case (Fig.2b) than the LP case (Fig.2a).

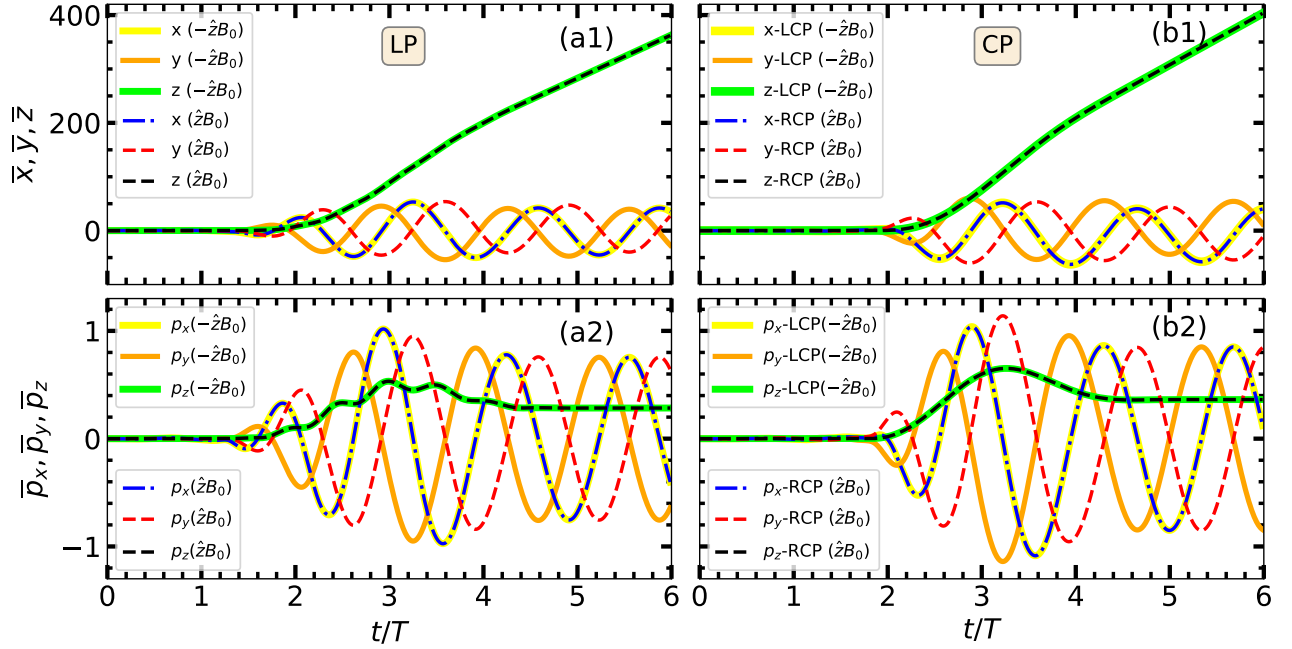


Figure 3. Time vs normalized position  $\bar{x}, \bar{y}, \bar{z}$  and normalized momentum  $\bar{p}_x, \bar{p}_y, \bar{p}_z$  of the RSM electron for LP (a1,a2) and CP (b1,b2) laser fields when  $\mathbf{B}_{ext} = \pm \hat{z}B_0$ . These trajectories correspond to those enhanced absorption cases of  $\bar{\mathcal{E}}_A \approx 13$  (LP case, blue, cyan lines in Fig.2a) and  $\bar{\mathcal{E}}_A \approx 17$  (CP case, yellow and red lines in Fig.2b) for  $I_0 = 1.83 \times 10^{17} \text{ W/cm}^2$  and  $B_0 = 0.057$  a.u. at ECR.

## 2. Phase dynamics of an electron with LP and CP laser field

To comprehend the enhancement of absorbed energy, it is important to analyze the temporal phase-angle dynamics between the velocity of the electron and the associated electric field. It is clear from Eq.(6) that the phase angle  $\Delta\psi$  between the electron velocity ( $\mathbf{v}$ ) and the driving electric field ( $\mathbf{E}$ ) plays crucial role to determine the rate of absorption  $d(\gamma m_0 c^2)/dt$ . When the phase angle  $\Delta\psi$  is an odd integral multiple of  $\pi/2$ , the rate of absorption is  $d(\gamma m_0 c^2)/dt = 0$ . However, the absorption rate becomes non-zero as  $\Delta\psi$  deviates from  $\pi/2$  (or odd integral multiple of  $\pi/2$ ) and it reaches maximum near  $\pi$  (or integral multiple of  $\pi$ ). In the case of the LP light, polarized along  $x$ -direction, the  $x$ -component of the field is dominant and  $d(\gamma m_0 c^2)/dt = qv_x E_x \approx qv_x E_l$  holds outside the cluster where space-charge field is negligible. In our earlier work<sup>34</sup>, by numerically retrieving the phase angles  $\psi_{v_x}, \psi_{E_x}$  of respective  $v_x, E_x$  and the phase difference  $\Delta\psi = \psi_{v_x} - \psi_{E_x}$  for a LP laser field, we demonstrated the importance of an ambient magnetic field  $\mathbf{B}_{ext} = +B_0 \hat{z}$  in the phase dynamics of an electron. Equation (6) indicates that, though  $B_{ext}$  does not have any direct impact on the energy absorption, it may re-orient the angle  $\psi_{v_x}$  and allow  $\Delta\psi$  to remain near  $\pi$  (or integral multiple of  $\pi$ ) for a prolonged duration which lead to a significant enhancement in energy absorption at ECR.

The phase-angle dynamics with LP laser field when  $\mathbf{B}_{ext} = -B_0 \hat{z}$  as well as CP laser fields with  $\mathbf{B}_{ext} = \pm B_0 \hat{z}$  have not been discussed yet. In Fig. 4a, we plot  $\Delta\psi = \psi_{v_x} - \psi_{E_x}$  for the LP laser field with  $\mathbf{B}_{ext} = \pm B_0 \hat{z}$  corresponding to the energy absorption curves (solid and dashed-dot) in Fig. 2a. In both the cases,  $\Delta\psi$  are maintained near  $\pi$  for the laser pulse

duration  $t/T \approx 1 - 2.5$  that lead to prominent increase in absorption in Fig.2a around this time. Also, the exact superposition of  $\Delta\psi$  values shows that the phase-angle dynamics for a LP laser field is unaltered irrespective of the direction of  $\mathbf{B}_{ext} = \pm B_0 \hat{z}$ . As a result, the energy absorption is also unaltered in Fig.2a irrespective of the direction of  $\mathbf{B}_{ext} = \pm B_0 \hat{z}$ .

In the case of LP laser field,  $\Delta\psi = \psi_{v_x} - \psi_{E_x}$  is calculated only for the laser polarization direction  $x$  in Fig.4a. However, for the CP case two different values of  $\Delta\psi = \psi_{v_x} - \psi_{E_x}$  and  $\Delta\psi = \psi_{v_y} - \psi_{E_y}$  are calculated due to two components of the driving CP fields. Hence, in Figs. 4b and 4c we show  $\psi_{v_x} - \psi_{E_x}$  and  $\psi_{v_y} - \psi_{E_y}$  for the LCP laser with  $\mathbf{B}_{ext} = -B_0 \hat{z}$  and for RCP laser with  $\mathbf{B}_{ext} = +B_0 \hat{z}$  corresponding to the  $\bar{\mathcal{E}}_A$  curves (solid light-grey and dashed-dot) in Fig. 2b respectively. In both cases, LCP with  $\mathbf{B}_{ext} = -B_0 \hat{z}$  and RCP with  $\mathbf{B}_{ext} = +B_0 \hat{z}$ , corresponding to  $\bar{\mathcal{E}}_A \sim 17$  in Fig.2b, we find  $\Delta\psi = \psi_{v_x} - \psi_{E_x}$  for the  $x$ -motion are exactly similar (solid lines) as shown in Figs. 4b and 4c. The dynamics of  $\Delta\psi = \psi_{v_y} - \psi_{E_y}$  for the  $y$ -motion are, however, different for both the cases (dashed lines in Figs. 4b,4c). One can identify that, when  $\Delta\psi = \psi_{v_x} - \psi_{E_x}$  deviates from  $\pi$  near  $t/T = 1.5$ , the other  $\Delta\psi = \psi_{v_y} - \psi_{E_y}$  still stays close to  $\pi$ . Until  $t/T \sim 2.8$  of the 5-cycle pulse, either one of the phase-angles or both remain close to  $\pi$ . Clearly, the combined effect of  $\psi_{v_x} - \psi_{E_x}$  and  $\psi_{v_y} - \psi_{E_y}$  for the CP lights allows net  $\Delta\psi$  to stay near  $\pi$  for a prolonged duration  $\approx 2.8$ -cycle from the beginning of the laser pulse. This improved phase matching in the case of CP fields lead to the further enhancement of  $\bar{\mathcal{E}}_A$  by  $\sim 4U_p$  compared to the LP laser field in Fig.2 in the end of the pulses. In the next section it is shown that  $\bar{\mathcal{E}}_A$  may enhance further by  $\sim 10 - 20U_p$  with CP laser.



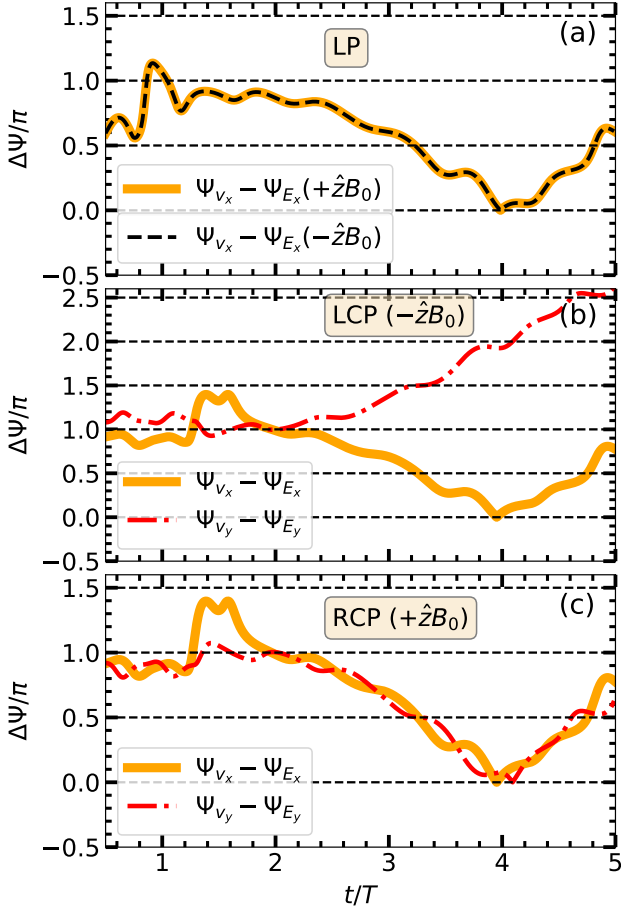


Figure 4. Phase dynamics  $\Delta\psi = \psi_{v_x} - \psi_{E_x}$  (for  $x$ -motion) and  $\Delta\psi = \psi_{v_y} - \psi_{E_y}$  (for  $y$ -motion) versus time are shown for the RSM electron in Fig.3. For LP case (a) with  $B_{ext} = -\hat{z}B_0$  (dash-dot lines) and  $B_{ext} = \hat{z}B_0$  (solid lines),  $\psi_{v_x} - \psi_{E_x}$  show exact match. For LCP field (c) with  $B_{ext} = -\hat{z}B_0$  and RCP field (b) with  $B_{ext} = \hat{z}B_0$ ,  $\psi_{v_x} - \psi_{E_x}$  show a good match (solid lines in b,c); but  $\psi_{v_y} - \psi_{E_y}$  are different (dash-dot lines in b,c). All parameters are same as in Fig.3.

## B. Particle-in-cell (PIC) simulation results

The results from RSM as described above in Sec.III A 1 gives a fundamental understanding of the physical process responsible for the higher absorption of laser energy by a cluster electron in the CP light. However, particle interactions can not be taken into account in this single-particle picture of the RSM. To treat the all kinds of particle-interactions starting from the creation of the nano-plasma self-consistently, we now use 3D-PIC simulation<sup>29,30,39,43-46</sup> as in the previous work<sup>34</sup>. The PIC code was upgraded for a hybrid method<sup>38</sup>, particularly to treat the electrons outside the computational box with MD simulations<sup>33,40</sup> to study the effect of ambient magnetic field on the energy absorption by the cluster electrons and propagation of these energetic electrons as a conical-spiral beam<sup>38</sup>. This upgraded PIC code is used for the present study where a deuterium cluster with  $R_0 = 2.2$  nm and number of atoms  $N = 2176$  is placed at the center of the simulation box. When the laser field  $\mathbf{E}_l(t)$  interacts with the neutral deuterium atoms, the ionization from D to D<sup>+</sup> happens via

the over-the-barrier ionization (OBI<sup>47</sup>) process as it reaches a critical field strength  $E_c = |\mathbf{E}_l(t)| = I_p^2(Z)/4Z$  (where,  $I_p(Z)$  stands for the ionization potential). Subsequently, the electrons and ions generated through OBI creates the coulomb field (or space charge field)  $\mathbf{E}_{sc}(\mathbf{r}, t) = -\nabla\phi(\mathbf{r}, t)$ , where  $\phi(\mathbf{r}, t)$  is the time-dependent potential that starts from zero. More details of the PIC code are given in Refs.<sup>29,30,34,38,39,43-46</sup>

A PIC ion/electron have the charge to mass ratio same as that of an actual ion/electron. Governing equation of motion in PIC simulation for the  $j$ -th electron and  $k$ -th ion is

$$\frac{d\mathbf{p}_{j|k}}{dt} = q_{j|k} [(\mathbf{E}_l(t) + \mathbf{E}_{sc}(\mathbf{r}_{j|k}, t)) + \mathbf{v}_{j|k} \times (\mathbf{B}_l + \mathbf{B}_{ext})] \quad (7)$$

$$\frac{d\mathbf{r}_{j|k}}{dt} = \mathbf{v}_{j|k} = \frac{\mathbf{p}_{j|k}}{\gamma_{j|k} m_{j|k}} \quad (8)$$

where  $\mathbf{p}_{j|k} = m_{j|k}\mathbf{v}_{j|k}\gamma_{j|k}$ ,  $\mathbf{v}_{j|k}$ ,  $\mathbf{r}_{j|k}$ ,  $m_{j|k}$ ,  $q_{j|k}$ ,  $\gamma_{j|k}$  represents momentum, velocity, position, mass, and charge of a PIC electron/ion respectively. Here,  $\gamma_{j|k} = \sqrt{1 + p_{j|k}^2/m_{j|k}^2 c^2}$  is the relativistic factor. In this case,  $m_j = m_0 = 1$ ,  $m_k = M_0 = 2 \times 1836$ ,  $q_j = -1$  and  $q_k = 1$  in a.u.. Initially, the charge density  $\rho_G$  is calculated and the Poisson's equation  $\nabla^2\phi_G = -\rho_G$  is solved on the numerical grids using time-dependent monopole boundary condition (subscript  $G$  represents grid values of charge density and potential). We then compute the corresponding potential  $\phi(\mathbf{r}_{j|k}, t)$  by interpolating  $\phi_G$  to the particle location. Further, by differentiating the interpolated  $\phi(\mathbf{r}_{j|k})$  analytically<sup>46</sup>, the electric field  $\mathbf{E}_{sc}(\mathbf{r}_{j|k}) = -\nabla\phi(\mathbf{r}_{j|k})$  is calculated at  $\mathbf{r}_{j|k}$ . The same laser fields (2) are employed in PIC and the same velocity verlet method (VVM) is used to solve the equations (7)-(8) as in RSM. Since, the laser field strength is high, we consider the collisionless interaction among electrons and ions. The sum of kinetic energy  $KE = \sum_l p_l^2/2m_l$  and potential energy  $PE = \sum_l q_l\phi_l$  of all electrons and ions leads to the total energy  $\mathcal{E}(t) = \sum_l q_l\phi_l + p_l^2/2m_l$  at time  $t$ . We also calculate the final average absorbed laser energy  $\mathcal{E}_A = \mathcal{E}(\tau)/N$  per electron in the end of the pulse at  $\tau = nT$  with  $n = 5$ -cycle. In the PIC simulation, it important to choose the numerical parameters (e.g. spatial and temporal resolution, grid size, number of PIC particles/cell etc.) correctly to avoid numerical heating. Typically, we take  $64^3, 128^3, 256^3$  grids (cells) of uniform cell size  $\Delta x = \Delta y = \Delta z = 16$  a.u., time step  $\Delta t = 0.1$  a.u., and approximately 15 particles/cell depending upon the cluster size.

### 1. PIC results and comparison with RSM

In the previous works<sup>34,38</sup>, we calculated the normalized absorbed energy  $\overline{\mathcal{E}}_A = \mathcal{E}_A/NU_p$  per electron for a range of  $B_0 = 0 - 2\omega$  with a LP laser field when  $\mathbf{B}_{ext} = +B_0\hat{z}$ . Using both PIC and RSM, we showed that  $\overline{\mathcal{E}}_A$  is not maximum at the ECR value of  $B_0 = \omega$ , instead the absorption peak occurred at a higher value of  $B_0$  beyond the ECR due to the relativistically modified ECR (RECR) condition,  $\Omega_c = \Omega_{c0}/\gamma = \omega$ . The same exercise is followed here for LP and CP (both RCP and LCP) laser fields with  $B_{ext} = \pm B_0\hat{z}$ , and  $\overline{\mathcal{E}}_A$  is calculated for different  $B_0$  values. Comparative results are shown in Figure 5. For the LP laser field with  $B_{ext} = \pm B_0\hat{z}$ , we find that

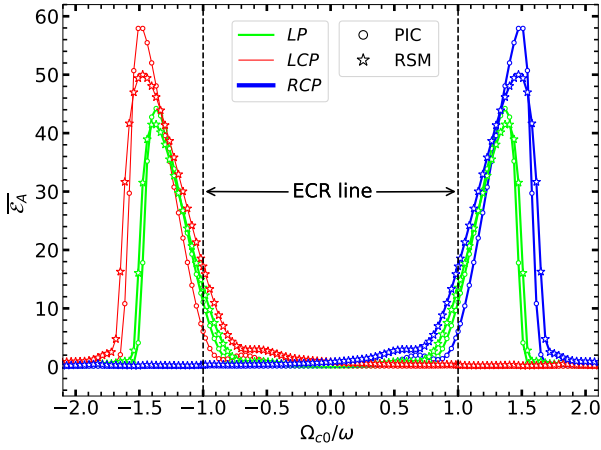


Figure 5. Comparison of normalized average absorbed energy  $\overline{\mathcal{E}}_A$  by a cluster electron for LP (green; light grey in grey scale) and CP laser field (blue and orange; black and dark grey in grey scale) in RSM ( $\star$ ) and PIC ( $\circ$ ) simulation within a range of  $B_{ext}$  when  $B_{ext} = \hat{z}B_0$  and  $B_{ext} = -\hat{z}B_0$ . The vertical dashed lines represents the ECR value of  $B_0 = 0.057$  a.u.. Other parameters are same as in Fig. 2.

$\overline{\mathcal{E}}_A$  is further enhanced from  $\approx 13$  (at ECR) to the maximum  $\approx 42$  for RSM (almost 3 times) and  $\approx 45$  for PIC at a shifted  $B_0$  value from the ECR (the vertical dashed lines in Fig. 5). The absorption curve of  $\overline{\mathcal{E}}_A$  show a mirror symmetry for LP laser field across  $B_{ext} = \pm B_0 \hat{z}$ . The single-electron RSM and the PIC results show a close matching.

In Fig. 5, we also show the RSM and PIC results for RCP and LCP laser fields with  $B_{ext} = \pm B_0 \hat{z}$  which are *central* to this work. Clearly, RCP with  $B_{ext} = -B_0 \hat{z}$  and LCP with  $B_{ext} = +B_0 \hat{z}$  leads to negligible  $\overline{\mathcal{E}}_A$  in both RSM and PIC. Conversely, RCP with  $B_{ext} = +B_0 \hat{z}$  and LCP with  $B_{ext} = -B_0 \hat{z}$  show maximum of  $\overline{\mathcal{E}}_A \approx 50, 59$  for RSM and PIC respectively. Thus absorption per electron  $\overline{\mathcal{E}}_A/N$  are  $\approx 8U_p, 14U_p$  higher compared to the respective LP cases (for RSM and PIC respectively). The absorption curves of  $\overline{\mathcal{E}}_A$  vs  $\Omega_{c0}/\omega$  with CP laser field also show a mirror symmetry in both PIC and RSM similar to the LP cases.

## 2. Angular distribution of PIC electrons

The energy and angular distributions of electrons are important for explaining their propagation as a beam. In an earlier report<sup>38</sup>, we discussed the energy and angular distribution of PIC and RSM electrons in both position and momentum space for a LP laser field with  $B_{ext} = +B_0 \hat{z}$ . The energetic electrons showed a narrow cone-like propagation as a weakly relativistic electron beam with an angular spread of  $\Delta\theta < 5^\circ$  at the ECR/RECR. In Figure 5, it is shown that a CP laser field leads to higher amount of absorption  $\sim 8U_p, 14U_p$  per electron (for RSM and PIC respectively) compared to the LP laser field. In this section, we focus on the angular distribution of these PIC electrons with CP laser fields and compare with the LP cases corresponding to the results in Fig.5.

In the position space the angular deflection of an electron ( $\theta_r$ ) is defined as, the angle made by the laser light while propagating along  $\mathbf{z}$  (similar to the direction of  $B_{ext} = B_0 \hat{z}$ ) with its

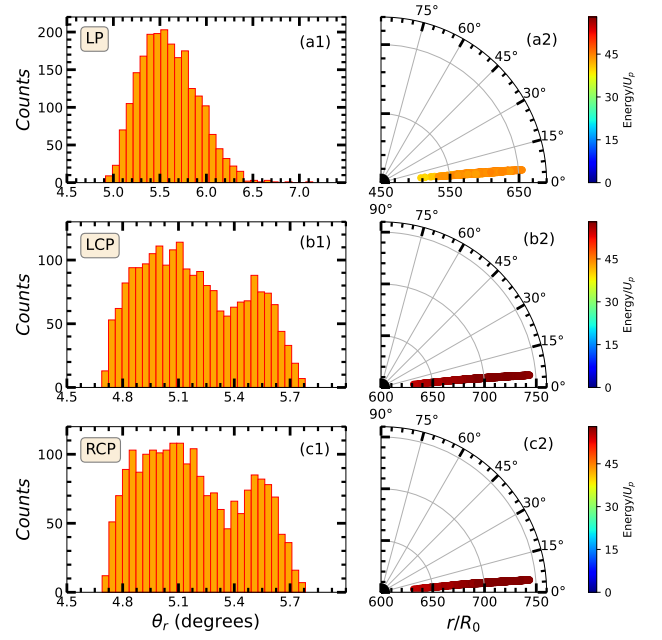


Figure 6. Histograms showing the angular distribution of PIC electrons in the position space  $\theta_r$  (left column) and respective polar plots with their normalized position  $r/R_0$  vs  $\theta_r$  (right column). These results correspond to the peak of the absorption curves in Fig.5 with  $B_0 = 0.079, 0.085$  a.u. for LP, CP respectively: LP with  $B_{ext} = -\hat{z}B_0$  (a1,a2), LCP with  $B_{ext} = -\hat{z}B_0$  (b1,b2), and RCP with  $B_{ext} = \hat{z}B_0$  (c1,c2). The polar co-ordinates ( $r, \theta_r$ ) are color-coded with their energy normalized by  $U_p$ . Other parameters are same as in Fig. 5.

position vector  $\mathbf{r}$ . This angle of elevation can be derived using

$$z = r \cos \theta_r, \quad r_\perp = r \sin \theta_r; \quad \text{here } r_\perp = \sqrt{x^2 + y^2}. \quad (9)$$

In Figure 6, we plot the histogram of PIC electrons vs.  $\theta_r$  (Fig. 6a1-6c1, left column) and the respective polar plots (Fig. 6a2-6c2, right column) of their normalized position  $r/R_0$  vs.  $\theta_r$  corresponding to the peak points of  $\overline{\mathcal{E}}_A$  curve in Figure 5. Polar co-ordinates ( $r, \theta_r$ ) are color-coded with the respective energy normalized by  $U_p$ . In the LP case, the electrons are spread over an angular range  $\theta_r \approx 5^\circ - 7^\circ$  with the angular spread  $\Delta\theta_r \sim 2^\circ$  (Fig.6a1) and the electron beam propagates to a distance  $r \approx 660R_0$  (Fig.6a2). However, with LCP and RCP the angular spread is further reduced to  $\Delta\theta_r \sim 1^\circ$  within an angular range  $\theta_r \approx 4.7^\circ - 5.7^\circ$  (Fig.6b1,6c1) and the propagation distance is increased to  $r \approx 750R_0$  (Fig.6b2,6c2). In all three cases, the electron beam makes a very narrow cone-angle  $\theta_r \approx 3^\circ - 4^\circ$  with respect to the magnetic field direction  $\mathbf{z}$ . This demonstrates that, with the CP laser field one may obtain energetically more intense electron beam of a very narrow angular spread  $\Delta\theta_r \sim 1^\circ$  compared to LP laser field.

The conical electron beam can also be elucidated by considering the angular deflection in the momentum space ( $\theta_p$ ) of the momentum vector  $\mathbf{p}$  w.r.t the laser propagation direction. This angle,  $\theta_p$ , often holds significance in determining the transport characteristics of electrons and the type of magnetic configuration needed to facilitate their transport as a beam. With transverse momentum ( $p_x, p_y$ ) and longitudinal

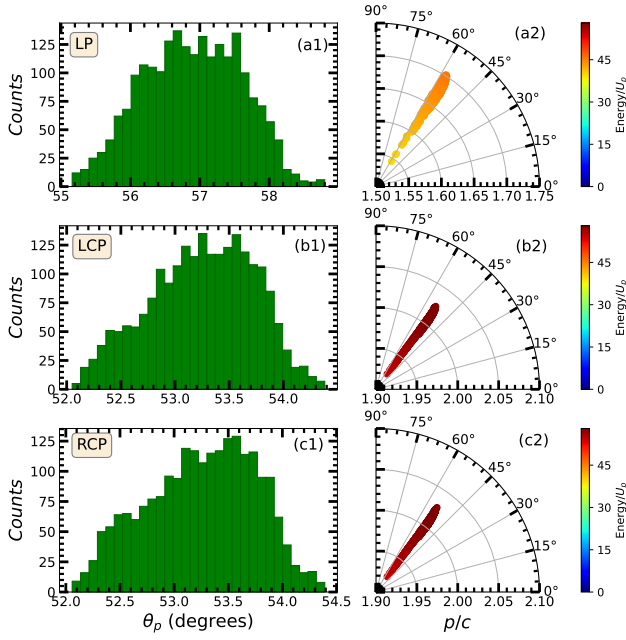


Figure 7. Histograms showing the angular distribution of PIC electrons in the momentum space  $\theta_p$  (left column) and respective polar plots with their normalized momenta  $p/c$  vs  $\theta_p$  (right column). The panels (a1,a2),(b1,b2), and (c1,c2) correspond to those panels (a1,a2), (b1,b2) and (c1,c2) in Fig.6 respectively. The polar coordinates ( $r, \theta_r$ ) are color-coded with their energy normalized by  $U_p$ . Other parameters are same as in Fig. 5.

momentum ( $p_z$ ), we calculate  $\theta_p$  from

$$p_z = p \cos \theta_p, p_\perp = p \sin \theta_p; \text{ where } p_\perp = \sqrt{p_x^2 + p_y^2}. \quad (10)$$

In Figure 7, we plot the histogram of PIC electrons vs.  $\theta_p$  (Fig.7a1-7c1, left column) and the respective polar plots (Fig.7a2-7c2, right column) of their normalized momentum  $p/c$  vs.  $\theta_p$  corresponding to Fig. 6 in the position space. Polar co-ordinates ( $p, \theta_p$ ) are color-coded with the respective energy normalized with  $U_p$ . In the LP case, the electrons are spread over an angular range  $\theta_p \approx 55^\circ - 59^\circ$  with an angular spread  $\Delta\theta_p \sim 4^\circ$  (Fig. 7a1). The momenta of the beam electrons reach weakly relativistic values  $p \approx 1.7c$  (Fig. 7a2) in LP. Again, with LCP and RCP the angular spread is reduced to  $\Delta\theta_p \sim 2^\circ$  within an angular range  $\theta_p \approx 52^\circ - 54^\circ$  (Fig. 7b1,7c1). The momentum of the beam electrons in these cases reach higher values of  $p \approx 2.03c$  (Fig. 7b2,7c2). In all three cases, the electron beams make wide cone-angles of  $\theta_p \approx 52^\circ - 55^\circ$  and propagate like a spiral conical beam with respect to the magnetic field direction  $z$ . This shows that, the CP case may produce energetically more intense electron beam of a very narrow angular spread  $\Delta\theta_p \sim 2^\circ$  of momentum compared to the LP case.

#### IV. SUMMARY

The goal of this work is to study the laser energy absorption by cluster electrons in the collisionless regime for CP laser pulses (both LCP and RCP) when external magnetic

fields  $\mathbf{B}_{ext} = \pm B_0 \hat{z}$  and with LP laser pulses for  $\mathbf{B}_{ext} = -B_0 \hat{z}$ ; which were not reported before. In earlier works<sup>34,38</sup>, we have shown that the interaction of 800 nm, 5-fs (FWHM) LP laser pulses for intensities  $I_0 = 7 \times 10^{16} - 2 \times 10^{17} \text{ W/cm}^2$  and  $\mathbf{B}_{ext} = +B_0 \hat{z}$  with  $B_0 = 0 - 2\omega$  a.u., enhances the average energy of a cluster electron  $\mathcal{E}_A \approx 36 - 70 U_p$ . This enhancement in  $\mathcal{E}_A$  is a two stage process<sup>34</sup> with anharmonic resonance (AHR) as the 1<sup>st</sup> stage and electron cyclotron resonance (ECR) or relativistic ECR (RECR) as the 2<sup>nd</sup> stage. In the present work, we show that the energy enhancement is unaltered when  $\mathbf{B}_{ext} = -B_0 \hat{z}$  with LP (Figs.2 and 5). But,  $\mathcal{E}_A$  is more than  $10 U_p$  (Fig.2 and Fig.5) higher with CP laser; particularly, when  $\mathbf{B}_{ext} = -B_0 \hat{z}$  for LCP and  $\mathbf{B}_{ext} = +B_0 \hat{z}$  for RCP (Fig.5). Otherwise, no further enhancement of  $\mathcal{E}_A$  occurs with  $\mathbf{B}_{ext} = \pm B_0 \hat{z}$ . Also, for both the LP and CP cases, the absorption curve with  $\mathbf{B}_{ext} = \pm B_0 \hat{z}$  show a mirror symmetry. The electrons propagate as a weakly relativistic electron beam (REB) in a conical-spiral having narrow opening angle of  $6^\circ - 7^\circ$  in the position space (Fig.6) and wide opening angle ( $55^\circ - 60^\circ$ ) in the momentum space (Fig.7) with respect to the laser propagation direction  $z$ . The angular spread of electrons  $\Delta\theta$  in both the position and the momentum space is  $\approx 4^\circ - 5^\circ$  with LP<sup>38</sup>. Present work shows that, the CP laser can further reduce the angular spread  $\Delta\theta \approx 2^\circ$  for both LCP and RCP with  $\mathbf{B}_{ext} = \pm B_0 \hat{z}$  respectively. We have also performed PIC simulations for bigger clusters of deuterium, argon and xenon (not shown here for conciseness) with CP laser pulses under similar conditions of this work, which show great enhancement of total absorption beyond the LP cases<sup>34,38</sup> and formation of more intense electron beams as shown in Figs.6 and 7.

Note that the field components of a CP light does not vanish simultaneously. In addition, the phase matching condition (Fig.4) shows that one of the field components (or both) of CP light may maintain the required phase with non-zero amplitude. This leads to higher absorption of the CP laser pulse than the LP case (Fig.2 and Fig.5) in presence of an ambient magnetic field. It also improves the quality of the emitted electron beam in terms of divergence and energy in CP than LP (Fig.6 and Fig.7).

This work may find importance for the fast ignition technique of inertial confinement fusion, laser-driven electron accelerators, and to understand energy absorption by plasma electrons as well as their dynamics under very strong field conditions in astrophysical environments, e.g., neutron stars and pulsars.

#### ACKNOWLEDGEMENTS

Authors acknowledge Dr. Sagar Shekhar Mahalik for the initial help in numerical simulations and fruitful discussion; and Dr. Sudip Sengupta for careful reading of the manuscript. The numerical simulations presented in this work have been performed using Antya Linux cluster of HPC facility at IPR.

#### REFERENCES

- 1T. Ditmire, J. W. G. Tisch, E. Springate, M. B. Mason, N. Hay, J. P. Marangos, and M. H. R. Hutchinson, Phys. Rev. Lett. **78**, 2732 (1997).

- <sup>2</sup>T. Ditmire, E. Springate, J. W. G. Tisch, Y. L. Shao, M. B. Mason, N. Hay, J. P. Marangos, and M. H. R. Hutchinson, *Phys. Rev. A* **57**, 369 (1998).
- <sup>3</sup>T. Ditmire, J. W. G. Tisch, E. Springate, M. B. Mason, N. Hay, J. Marangos, and M. H. R. Hutchinson, *Nature (London)* **386**, 54 (1997).
- <sup>4</sup>M. Lezius, S. Dobosz, D. Normand, and M. Schmidt, *Phys. Rev. Lett.* **80**, 261 (1998).
- <sup>5</sup>R. Rajeev, T. M. Trivikram, K. P. M. Rishad, V. Narayanan, E. Krishnakumar, and M. Krishnamurthy, *Nat Phys.* **9**, 185 (2013).
- <sup>6</sup>L. M. Chen, J. J. Park, K. H. Hong, I. W. Choi, J. L. Kim, J. Zhang, and C. H. Nam, *Physics of Plasmas* **9**, 3595 (2002).
- <sup>7</sup>Y. L. Shao, T. Ditmire, J. W. G. Tisch, E. Springate, J. P. Marangos, and M. H. R. Hutchinson, *Phys. Rev. Lett.* **77**, 3343 (1996).
- <sup>8</sup>E. Springate, S. A. Aseyev, S. Zamith, and M. J. J. Vrakking, *Phys. Rev. A* **68**, 053201 (2003).
- <sup>9</sup>L. M. Chen, J. J. Park, K.-H. Hong, J. L. Kim, J. Zhang, and C. H. Nam, *Phys. Rev. E* **66**, 025402 (2002).
- <sup>10</sup>A. McPherson, B. D. Thompson, A. B. Borisov, K. Boyer, and C. K. Rhodes, *Nature* **370**, 631 (1994).
- <sup>11</sup>L. M. Chen, F. Liu, W. M. Wang, M. Kando, J. Y. Mao, L. Zhang, J. L. Ma, Y. T. Li, S. V. Bulanov, T. Tajima, Y. Kato, Z. M. Sheng, Z. Y. Wei, and J. Zhang, *Phys. Rev. Lett.* **104**, 215004 (2010).
- <sup>12</sup>J. Jha, D. Mathur, and M. Krishnamurthy, *Journal of Physics B: Atomic, Molecular and Optical Physics* **38**, L291 (2005).
- <sup>13</sup>F. Dorchie, T. Caillaud, F. Blasco, C. Bonté, H. Jouin, S. Micheau, B. Pons, and J. Stevefelt, *Phys. Rev. E* **71**, 066410 (2005).
- <sup>14</sup>V. Kumarappan, M. Krishnamurthy, D. Mathur, and L. C. Tribedi, *Phys. Rev. A* **63**, 023203 (2001).
- <sup>15</sup>C. Rose-Petruck, K. J. Schafer, K. R. Wilson, and C. P. J. Barty, *Phys. Rev. A* **55**, 1182 (1997).
- <sup>16</sup>D. Bauer and A. Macchi, *Phys. Rev. A* **68**, 033201 (2003).
- <sup>17</sup>C. Siedschlag and J. M. Rost, *Phys. Rev. A* **67**, 013404 (2003).
- <sup>18</sup>E. M. Snyder, S. A. Buzza, and A. W. Castleman, Jr., *Phys. Rev. Lett.* **77**, 3347 (1996).
- <sup>19</sup>K. Ishikawa and T. Blenski, *Phys. Rev. A* **62**, 063204 (2000).
- <sup>20</sup>F. Megi, M. Belkacem, M. A. Bouchene, E. Suraud, and G. Zwicknagel, *Journal of Physics B: Atomic, Molecular and Optical Physics* **36**, 273 (2003).
- <sup>21</sup>C. Jungreuthmayer, L. Ramunno, J. Zanghellini, and T. Brabec, *IOP Publishing* **38**, 3029 (2005).
- <sup>22</sup>D. Bauer, *Journal of Physics B: Atomic, Molecular and Optical Physics* **37**, 3085 (2004).
- <sup>23</sup>T. Ditmire, T. Donnelly, A. M. Rubenchik, R. W. Falcone, and M. D. Perry, *Phys. Rev. A* **53**, 3379 (1996).
- <sup>24</sup>I. Last and J. Jortner, *Phys. Rev. A* **60**, 2215 (1999).
- <sup>25</sup>U. Saalmann and J.-M. Rost, *Phys. Rev. Lett.* **91**, 223401 (2003).
- <sup>26</sup>T. Fennel, G. F. Bertsch, and K.-H. Meiwes-Broer, *The European Physical Journal D - Atomic, Molecular, Optical and Plasma Physics* **29**, 367 (2004).
- <sup>27</sup>P. Mulser and M. Kanapathipillai, *Phys. Rev. A* **71**, 063201 (2005).
- <sup>28</sup>P. Mulser, M. Kanapathipillai, and D. H. H. Hoffmann, *Phys. Rev. Lett.* **95**, 103401 (2005).
- <sup>29</sup>M. Kundu and D. Bauer, *Phys. Rev. A* **74**, 063202 (2006).
- <sup>30</sup>M. Kundu and D. Bauer, *Phys. Rev. Lett.* **96**, 123401 (2006).
- <sup>31</sup>I. Kostyukov and J.-M. Rax, *Phys. Rev. E* **67**, 066405 (2003).
- <sup>32</sup>T. Taguchi, T. M. Antonsen, and H. M. Milchberg, *Phys. Rev. Lett.* **92**, 205003 (2004).
- <sup>33</sup>S. S. Mahalik and M. Kundu, *Physics of Plasmas* **23**, 123302 (2016).
- <sup>34</sup>K. Swain, S. S. Mahalik, and M. Kundu, *Scientific Reports* **12**, 11256 (2022).
- <sup>35</sup>P. Moreno, L. Plaja, and L. Roso, *Europhysics Letters (EPL)* **28**, 629 (1994).
- <sup>36</sup>P. Moreno, L. Plaja, and L. Roso, *Phys. Rev. A* **55**, R1593 (1997).
- <sup>37</sup>M. Lein and J. M. Rost, *Phys. Rev. Lett.* **91**, 243901 (2003).
- <sup>38</sup>K. Swain, S. S. Mahalik, and M. Kundu, *Phys. Rev. A* **108**, 053104 (2023).
- <sup>39</sup>M. Kundu, P. K. Kaw, and D. Bauer, *Phys. Rev. A* **85**, 023202 (2012).
- <sup>40</sup>S. S. Mahalik and M. Kundu, *Phys. Rev. A* **97**, 063406 (2018).
- <sup>41</sup>S. R. Krishnan, L. Fechner, M. Kremer, V. Sharma, B. Fischer, N. Camus, J. Jha, M. Krishnamurthy, T. Pfeifer, R. Moshhammer, J. Ullrich, F. Stienke-meier, M. Mudrich, A. Mikaberidze, U. Saalmann, and J.-M. Rost, *Phys. Rev. Lett.* **107**, 173402 (2011).
- <sup>42</sup>S. R. Krishnan, R. Gopal, R. Rajeev, J. Jha, V. Sharma, M. Mudrich, R. Moshhammer, and M. Krishnamurthy, *Phys. Chem. Chem. Phys.* **16**, 8721 (2014).
- <sup>43</sup>M. Kundu, S. V. Popruzhenko, and D. Bauer, *Phys. Rev. A* **76**, 033201 (2007).
- <sup>44</sup>S. V. Popruzhenko, M. Kundu, D. F. Zaretsky, and D. Bauer, *Phys. Rev. A* **77**, 063201 (2008).
- <sup>45</sup>M. Kundu and D. Bauer, *Physics of Plasmas* **15**, 033303 (2008).
- <sup>46</sup>M. Kundu, *Energy absorption, ionization, and harmonic emission in laser-irradiated atomic clusters*, Ph.D. thesis, Ruprecht-Karls-Universität, Heidelberg (2007).
- <sup>47</sup>H. Bethe and E. Salpeter, *Quantum Mechanics of One and Two Electron Atoms* (Springer, Berlin, 1957).